Complex-Hamiltonian paraxial description of damped geodesic acoustic modes

E. Poli[1,*], F. Palermo[1], A. Bottino[1], O. Maj[1], H. Weber[1]

[1] *Max-Planck-Institut für Plasmaphysik, 85748 Garching bei München, Germany*

[*] Corresponding author: emanuele.poli@ipp.mpg.de

Abstract: Geodesic acoustic modes (GAMs) are a fundamental part of turbulence and zonal-flow dynamics in tokamaks. They exhibit simple yet non-trivial dispersive and dissipative properties. In linear numerical simulations, they are often initialized in the form of (e.g. Gaussian) packets which evolve in time. Depending on the parameters, dispersion and damping can act on comparable time scales during the GAM evolution. Wigner-function methods developed in the frame of non-Hermitian quantum mechanics are shown to be applicable to damped geodesic oscillations. In this approach, the standard approximation of "weak damping", often introduced for the treatment of plasma waves, is not needed. The method requires that the properties of the plasma do not vary significantly across the width of the packet (i.e. in the radial direction), so that a paraxial expansion of the underlying equations around the centre of the packet can be applied. For a quadratic Hamiltonian, the equations for the Wigner function governing the packet in the paraxial limit are shown to be equivalent to the equations of paraxial WKB theory (usually applied to the description of high-frequency wave beams in plasmas), with the real Hamiltonian replaced by the corresponding complex one. Analytic solutions are derived in particular cases and shown to agree with the results of global gyrokinetic simulations.

Keywords: Plasma physics, magnetic confinement, WKB approximation, complex eikonal, geodesic acoustic modes

1 Introduction

Geodesic Acoustic Modes (GAMs) are axisymmetric plasma oscillations originating from the fact that zonal $\mathbf{E} \times \mathbf{B}$ flows are not divergence-free in tokamak geometry. Their compression leads to an oscillation, first described by Winsor *et al.* [1] using the equations of magnetohydrodynamics, which has a typical frequency of the order of the sound speed divided by the major radius of the tokamak. Since this seminal work, the interest in GAMs increased considerably, in particular in the context of the dynamics of turbulence and zonal flows [2, 3, 4, 5], as reviewed in [6]. The theoretical treatment was further refined by including finite-β and collisionality effects in fluid analyses [7, 8]. A variety of kinetic effects is also crucial for the GAM excitation, dispersion and damping and the interested reader is referred to [9] for a compact overview. In particular, the importance of a kinetic treatment of the electrons was discussed e.g. in [10, 11, 12, 13, 14, 15]. Meanwhile, gyrokinetic simulations can be considered as a standard tool to tackle both linear and nonlinear GAM-related problems [16, 17, 18, 19, 20, 21].

Due to their role in turbulence regulation, a significant body of work on GAMs is available on the experimental side as well, see e.g. [22, 23, 24, 25, 26, 27, 28, 29, 30] and references therein.

The linear properties of the GAM oscillation, which are of particular relevance for this paper, and primarily the GAM dispersion relation, have been investigated in detail in a kinetic frame in e.g. [31, 32, 33]. In this context, also the radial propagation of the GAM has been investigated [34, 35, 36, 37], including the role of the nonlinear drive [38]. An important aspect of the GAM dynamics is that they can be heavily (Landau) damped, this

damping being dependent on various parameters and notably on the radial wavevector k_r through finite-orbit effects [31, 16, 39].

The relatively simple nature of the GAM oscillation, and the possibility of studying it–at least theoretically–as a radially localized wave packet, make it a well-suited test-bed for the application of paraxial techniques, which in the context of nuclear fusion are mainly applied to the description of focused and/or collimated wave beams used for plasma heating, see e.g. [40, 41, 42] and particularly [43, 44, 45, 46], where an approach very close to that of this paper is adopted. In this respect, it should be stressed that low-frequencies eigenmodes in tokamaks (which include non-Hermitian dispersion functions of interest in this paper, see below) can be described in terms of propagating wave packets as well, see [47] and references therein, a method which can be applied when the group-velocity component perpendicular to the magnetic field is much smaller than that in parallel direction, like in the case of lower hybrid waves [48]. A complex generalization of this approach has been proposed to capture asymmetries in the two-dimensional structure of the eigenmode [49]. Interestingly, also the paraxial WKB method mentioned above were applied to low-frequency eigenmodes in early work [50].

Specifically for the description of the linear evolution of GAMs, in the past years methods of (complex) geometrical optics have been considered successfully in [36, 37]. In particular, it was shown that the radial dependence of the plasma parameters (temperature in particular) leads to an evolution in time of k_r, which impacts both the dispersive and the dissipative properties of the oscillation, leading to a radial displacement of the packet on one side and to an enhanced damping on the other side [51, 52].

In the papers quoted above [36, 37], the focus was on the dispersive properties of the oscillation rather than on dissipation. Less than a decade ago, a theoretical description of the evolution of Gaussian packets subject to significant damping has been developed in the frame of the semiclassical (WKB) analysis of coherent quantum states in non-Hermitian Hamiltonian systems [53, 54], based on the Wigner-function formalism. Since a paraxial wave equation possesses the same form as the Schrödinger equation, it can be surmised that a similar approach can be applied also to problems of plasma physics, provided that the packet is sufficiently localized in space so that a paraxial expansion is justified. Interestingly, while the Wigner-function formalism gives a description of the wave through real equations in phase space, an equivalent description (at least for quadratic Hamiltonians) can be obtained in configuration space in terms of a complex WKB formalism, as shown in [54]. The corresponding equations coincide with those of the paraxial WKB method as developed for the propagation of high-frequency wave beams in plasmas [43, 44], with two fundamental differences. First, the "coordinate along the ray path", which is a space coordinate in wave-beam applications, is replaced by the time in the case of wave packets. Second, the Hamiltonian employed to trace the packet becomes complex, while in plasma applications the Hamiltonian is real and absorption does not influence the beam propagation, but appears as a damping on the trajectory determined through the real Hamiltonian (or in other words through the Hermitian part of the dielectric tensor). The equivalence of the two methods, which can be checked by explicit calculation, has its roots in the structure of the underlying equations; the reader is referred to [54] for more details.

The main goal of this paper is to demonstrate the applicability of the approach developed in [53, 54] outside quantum mechanics, considering the simple case of the GAM oscillation in a tokamak. The results obtained through either the (complex) paraxial WKB or the Wigner-function approaches are shown to agree very well with numerical gyrokinetic simulations, which entail a more complete description of the GAM physics. After a brief introduction on the basic properties of the GAM dispersion relation (Sec. 2), the relevant paraxial equations are discussed in Sec. 3 and explicit analytic solutions are derived in particular cases in Sec. 4 and 5. The solutions obtained with both methods mentioned above are shown to be equivalent. The width of the GAM packet is found to be characterized by two typical time scales, the dispersion leading to a time constant t_R which is the equivalent of the Rayleigh range in optics, and dissipation leading to a diffusion

time t_D, for which a simple physics interpretation is given. The analytic predictions are compared to linear gyrokinetic simulations performed with the global particle-in-cell code ORB5 [55, 56, 57] in Sec. 6. Conclusions are drawn in Sec. 7. Appendix A provides a summary of some basic definitions related to the Wigner-Weyl approach, while the derivation of the paraxial equations is reviewed in Appendix B and the relation between the Gaussian-envelope descriptions in both methods is briefly discussed in Appendix C.

2 The dispersion relation of Geodesic Acoustic Modes

The dynamics of a Gaussian GAM packet can be treated in the frame of paraxial theory, provided that its radial extension is smaller than the region over which the plasma parameter vary significantly. The GAM dispersion relation will be taken in the form (see e.g. [33] and references therein):

$$\omega = \omega_0 \left(1 + \frac{1}{2}\alpha_1 k_r^2 \rho_i^2\right), \tag{1}$$

with

$$\omega_0 = \left[1 + \frac{2(23 + 16\tau_e + 4\tau_e^2)}{q^2(7 + 4\tau_e)}\right]^{1/2} \left(\frac{7}{4} + \tau_e\right)^{1/2} \frac{v_{\mathrm{th},i}}{R_0}. \tag{2}$$

In the previous equation, $\tau_e = T_e/T_i$ is the electron-to-ion temperature ratio, R_0 is the major radius of the tokamak, ρ_i is the ion Larmor radius and α_1 is a τ_e-dependent coefficient of order one [32, 33] which changes sign around $\tau_e \approx 6$,

$$\alpha_1 = \frac{1}{2}\left[\frac{3}{4} - \left(\frac{7}{4} + \tau_e\right)^{-1}\left(\frac{13}{4} + 3\tau_e + \tau_e^2\right) + \left(\frac{7}{4} + \tau_e\right)^{-2}\left(\frac{747}{32} + \frac{481}{32}\tau_e + \frac{35}{8}\tau_e^2 + \frac{\tau_e^3}{2}\right)\right]. \tag{3}$$

In a homogeneous medium, the ion thermal speed $v_{\mathrm{th},i}$ and the safety factor q are constant, otherwise they are a function of the minor-radius coordinate r. In the cases studied here, $k_r\rho_i \ll 1$ for k_r within the spectral width of the packet. This limit has been used to Taylor-expand the square root in the last factor in Eq. (1).

For the GAM damping rate, we employ a useful formula [31] which takes into account lowest-order finite-orbit-width corrections in the limit $k_r\rho_i \ll 1/q^2 \ll 1$:

$$\begin{aligned}\gamma &= \frac{q^2\sqrt{\pi}}{2}\frac{v_{\mathrm{th},i}}{qR_0}\left[1 + \frac{2(23 + 16\tau_e + 4\tau_e^2)}{q^2(7 + 4\tau_e)}\right]^{-1}\left\{\left[\hat{\omega}_G^4 + (1 + 2\tau_e)\hat{\omega}_G^2\right]\exp\left(-\hat{\omega}_G^2\right)\right. \\ &+ \left.\frac{1}{4}\left[\frac{\hat{\omega}_G^6}{128} + \frac{1 + \tau_e}{16}\hat{\omega}_G^4 + \left(\frac{3}{8} + \frac{7\tau_e}{16} + \frac{5\tau_e^2}{32}\right)\hat{\omega}_G^2\right]\exp\left(-\hat{\omega}_G^2/4\right)\left(\frac{q v_{\mathrm{th},i} k_r}{\Omega_i}\right)^2\right\},\end{aligned} \tag{4}$$

where $\hat{\omega}_G = qR_0\omega_0/v_{\mathrm{th},i}$. Here and in the following, to draw a clearer connection with previous work [53, 54], we take the convention that positive values of γ correspond to damping. Hence, the imaginary part of the dispersion relation exhibits a similar functional dependence on the variables r and k_r as the real part of the dispersion relation (1) which allows us to write for the *complex* frequency $\overline{\omega} = \omega - i\gamma = \mathcal{F}(r) + \mathcal{G}(r)k_r^2/2$, where the complex functions $\mathcal{F}$ and $\mathcal{G}$ account for the dependences expressed by Eq. (1) for the real part and Eq. (4) for the imaginary part of $\overline{\omega}$. Although more complete expressions for the GAM dispersion relation are available in the literature, see for example [32], in this paper we will use the relatively simple expressions (1,4) reported above. This has basically two reasons. One the one side, it has been shown in [36] that these expressions are in good agreement with numerical simulations (at least for the parameters we will consider, see also discussion in Sec. 6). Secondly, this choice for the dispersion relation (i.e. for the Hamiltonian used below), which is a polynomial of second degree in the wavevector coordinate k_r, simplifies considerably the analysis presented in Sec. 4 and 5 and allows us to compare directly the Wigner-function approach with the complex paraxial WKB method, as mentioned in Sec. 1.

3 Paraxial equations

The derivation of the paraxial equations for both the radial electric field and the corresponding Wigner function is reviewed in Appendix B. In this section, we report and briefly comment the resulting equations, which are later applied to the case of GAM oscillations.

The equations for the evolution of the GAM packet follow from the Hamiltonian

$$\overline{H} = H - i\Gamma = \mathcal{F}(r) + \frac{1}{2}\mathcal{G}(r)k_r^2 = \omega - i\gamma \tag{5}$$

with the complex functions $\mathcal{F}$ and $\mathcal{G}$ introduced above. No assumption about the size of Γ as compared to H is made. As noted above, only the radial coordinate r appears in Eq. (5) i.e. the system is one-dimensional in space (and the corresponding phase-space two-dimensional). The strong analogy between the treatment developed in the following and the propagation of a wave beam relies on the fact that in both cases the evolution of the wave can be tracked through a "parameter along the beam trajectory", which in the present case is related explicitly to time rather than to space, as mentioned in Sec. 1 and discussed below.

3.1 Paraxial WKB equations

The paraxial WKB (pWKB) method looks for a solution of the relevant wave equation in the form

$$\psi(t,r) = A(t)e^{i[k_0(t)(r-r_0(t))+\frac{1}{2}\overline{s}(t)(r-r_0(t))^2]-i\,\overline{\omega}t}. \tag{6}$$

The centre (k_0, r_0) of the packet obeys equations (B.7) derived in Appendix B:

$$\frac{\mathrm{d}r_0}{\mathrm{d}t} = \overline{H}_k \qquad\qquad \frac{\mathrm{d}k_0}{\mathrm{d}t} = -\overline{H}_r, \tag{7}$$

while its transverse structure follows Eq. (B.8)

$$\frac{\mathrm{d}\overline{s}}{\mathrm{d}t} = -\overline{H}_{rr} - 2\overline{H}_{kr}\overline{s} - \overline{H}_{kk}\overline{s}^2, \tag{8}$$

which is a complex Riccati equation for the beam envelope $\overline{s} = s + i\phi$. Here, $\phi > 0$ is related to the width w of the packet by $\phi(t) = 2/w^2(t)$, while s is connected to the curvature of the wave front in the (t, r) space. In the previous equations, partial differentiation with respect to a given variable is indicated by the corresponding subscript. Finally the equation (B.9) for the amplitude reads

$$\frac{\mathrm{d}A}{\mathrm{d}t} = A\left[i\left(k_0\frac{\mathrm{d}r_0}{\mathrm{d}t}\right) - \frac{1}{2}\frac{\mathrm{d}\overline{H}_k}{\mathrm{d}r}\right], \tag{9}$$

where the last term is related to the divergence of the group velocity, with $\mathrm{d}\overline{H}_k/\mathrm{d}r = \overline{H}_{kr} + \overline{H}_{kk}\overline{s}$. The equation for the complex amplitude $A = |A|\exp(i\varphi)$ can be split into the following two equations

$$\frac{\mathrm{d}|A|}{\mathrm{d}t} = -\frac{1}{2}\mathrm{Re}\left[\frac{\mathrm{d}\overline{H}_k}{\mathrm{d}r}\right]\ |A| \tag{10}$$

$$\frac{\mathrm{d}\varphi}{\mathrm{d}t} = -\frac{1}{2}\mathrm{Im}\left[\frac{\mathrm{d}\overline{H}_k}{\mathrm{d}r}\right]. \tag{11}$$

Note that the paraxial theory as derived by Pereverzev from an asymptotic analysis of the Maxwell equations is valid for "weak" absorption, i.e. the anti-Hermitian part of the dielectric tensor is ordered small (by a factor $\kappa^{-1} \equiv c/\omega L \ll 1$) with respect to the Hermitian part [44] (here c is the speed of light and L the inhomogeneity scale of the medium). In the derivation presented in Appendix B, no assumption concerning the imaginary part of H has been made. For this reason the dissipation does not appear explicitly on the right-hand side of Eq. (9). This point is addressed further in Sec. 4.4.

3.2 Paraxial Wigner function

In Appendix B, the evolution equations for the Wigner transform of a Gaussian packet are derived following [53]. The result is a set of paraxial equations for the quantities z_0, G and α which appear in $W(z,t) \sim \alpha(t)\exp[-(z-z_0(t))\cdot G(t)(z-z_0(t))-2\gamma t]$, where $z=(k_r,r)$ is the phase-space variable associated to the radial direction, and the symmetric matrix G is related to the Gaussian parameters s and ϕ used above by (see Appendix C)

$$G = \begin{pmatrix} G_{kk} & G_{kr} \\ G_{kr} & G_{rr} \end{pmatrix} = \begin{pmatrix} 1/\phi & -s/\phi \\ -s/\phi & s^2/\phi+\phi \end{pmatrix} \tag{12}$$

The (real) equations to be solved for a reconstruction of the wave packet read for the centre of the packet (they reduce to the standard Hamilton equations for $\Gamma \to 0$):

$$\frac{\mathrm{d}k_0}{\mathrm{d}t} = -H_r - \Gamma_k G_{rr} + \Gamma_r G_{kr} \tag{13}$$

$$\frac{\mathrm{d}r_0}{\mathrm{d}t} = H_k + \Gamma_k G_{kr} - \Gamma_r G_{kk} \tag{14}$$

for the Gaussian envelop (G matrix):

$$\frac{\mathrm{d}G}{\mathrm{d}t} = \begin{pmatrix} 2H_{kr}G_{kk} - 2H_{kk}G_{kr} & -H_{kk}G_{rr} + H_{rr}G_{kk} \\ -H_{kk}G_{rr} + H_{rr}G_{kk} & 2H_{rr}G_{kr} - 2H_{kr}G_{rr} \end{pmatrix} + \tag{15}$$

$$\begin{pmatrix} \Gamma_{kk}(1-G_{kr}^2) + 2\Gamma_{kr}G_{kk}G_{kr} - \Gamma_{rr}G_{kk}^2 & \Gamma_{kr}(1+G_{kr}^2+G_{kk}G_{rr}) - \Gamma_{kk}G_{kr}G_{rr} - \Gamma_{rr}G_{kk}G_{kr} \\ \Gamma_{kr}(1+G_{kr}^2+G_{kk}G_{rr}) - \Gamma_{kk}G_{kr}G_{rr} - \Gamma_{rr}G_{kk}G_{kr} & \Gamma_{rr}(1-G_{kr}^2) + 2\Gamma_{kr}G_{kr}G_{rr} - \Gamma_{kk}G_{rr}^2 \end{pmatrix}$$

and for the amplitude:

$$\frac{1}{\alpha}\frac{\mathrm{d}\alpha}{\mathrm{d}t} = -\frac{1}{2}\left(\Gamma_{rr}G_{kk} - 2\Gamma_{kr}G_{kr} + \Gamma_{kk}G_{rr}\right). \tag{16}$$

Since we single out the dependence on the (complex) frequency in the Gaussian ansatz, the term -2Γ which appears on the right-hand side of the amplitude equation in [53] does not appear in Eq. (16).

It is shown below that both the pWKB method and the Wigner-function approach lead to the same results, if the initial conditions are chosen consistently. It is interesting to note that only two of the three equations (15) for the symmetric matrix G are needed in order to reconstruct the two physical quantities s and ϕ (or the complex quantity $\overline{s}$) of pWKB theory. As noted first by Littlejohn, this redundancy in the Wigner-function approach appears to be related to the fact that "Wigner functions are capable of representing both pure and mixed states" [58] (while the Schrödinger equation for the wavefunction ψ can describe only pure states). In classical physics, mixed states can arise e.g. through beam scattering from density fluctuations [59] and their "purity" can be quantified through an appropriate entropy function [60]. Here, this redundancy is exploited to reduce the number of equations to be solved, as reported in the next sections.

In the following, a few cases are discussed for which analytic solutions for both the paraxial WKB equations and those of the Wigner-function approach can be derived.

4 Homogeneous plasma

If the background plasma is spatially uniform, all the derivatives with respect to the radial coordinate r in the previous equations vanish and the problem has simple analytic solutions.

4.1 Paraxial WKB approach, no damping

We consider first the case of negligible damping, so that the Hamiltonian is real. In the case of a uniform plasma, the equation for the maximum of the packet imply $r = r_0$ and $k_r = k_0 = 0$. Eq. (8) reduces to

$$\frac{\mathrm{d}\overline{s}}{\mathrm{d}t} = -H_{kk}\overline{s}^2, \tag{17}$$

where $H_{kk} = \omega_0\alpha_1\rho_i^2$ is a constant. This equation can be solved straightforwardly by separation of variables. One has

$$\frac{1}{\overline{s}} - \frac{1}{\overline{s}_0} = H_{kk}t \tag{18}$$

with the final result [61, 37]

$$\overline{s}(t) = \frac{\overline{s}_0}{1 + H_{kk}\overline{s}_0 t}. \tag{19}$$

Splitting real and imaginary part yields explicitly

$$s(t) = \frac{s_0 + H_{kk}\left(s_0^2 + \phi_0^2\right)t}{\left(1 + H_{kk}s_0 t\right)^2 + H_{kk}^2\phi_0^2 t^2}, \qquad \phi(t) = \frac{\phi_0}{\left(1 + H_{kk}s_0 t\right)^2 + H_{kk}^2\phi_0^2 t^2} \tag{20}$$

Assuming no initial "focusing" of the packet ($s_0 = 0$), the initial condition is $\overline{s}_0 = i\phi_0 = 2i/w_0^2$ so that the solution for the evolving width of the packet is

$$\phi(t) = \mathrm{Im}[\overline{s}] = \frac{\phi_0}{1 + \omega_0^2\alpha_1^2\rho_i^4\phi_0^2 t^2} \tag{21}$$

or, taking the relation between ϕ and w into account,

$$w^2(t) = w_0^2\left[1 + \left(\frac{2\omega_0\alpha_1\rho_i^2 t}{w_0^2}\right)^2\right]. \tag{22}$$

This well-known expression describing the broadening of a wave packet in the presence of dispersion (notice that broadening occurs for both positive and negative values of α_1) allows the identification of a "Rayleigh time" by analogy with the treatment of wave beams in optics [37], namely

$$t_R = \frac{1}{H_{kk}\phi_0} = \frac{w_0^2}{2\omega_0\alpha_1\rho_i^2} \tag{23}$$

(we choose here to include the sign of α_1 in the definition of t_R) and write

$$w(t) = w_0\sqrt{1 + \frac{t^2}{t_R^2}}. \tag{24}$$

The curvature of the wave front is given by the real part of $\overline{s}$ and reads for the same initial conditions

$$s(t) = \mathrm{Re}[\overline{s}] = \frac{\omega_0\alpha_1\rho_i^2\phi_0^2 t}{1 + \omega_0^2\alpha_1^2\rho_i^4\phi_0^2 t^2} \tag{25}$$

or, in terms of the Rayleigh time,

$$s(t) = \frac{2}{w_0^2}\frac{t/t_R}{1 + t^2/t_R^2}. \tag{26}$$

Note that the sign of this term does depend on the sign of α_1, giving rise to both "normal" (for $\alpha_1 < 0$) and "anomalous" (for $\alpha_1 > 0$) phase fronts, using the terminology of [62], as shown in [37] and in Sec. 6.

The equation for the amplitude can also be integrated in a straightforward way. Since without damping the Hamiltonian is real, and since in the homogeneous case $H_{kr} = 0$, one

has Re[div (H_k)] = $H_{kk}s$ and Im[div (H_k)] = $H_{kk}\phi$, with div (H_k) defined in Eq. (B.10). Integration of Eq. (10) with $s(t)$ given by Eq. (26) yields with the help of Eq. (23)

$$\log \frac{|A(t)|}{|A_0|} = -\frac{1}{4}\log\left[1+\frac{t^2}{t_R^2}\right] \Rightarrow |A(t)| = \sqrt{\frac{w_0}{w(t)}}\,|A_0| \tag{27}$$

while integration of Eq. (11) with $\phi(t)$ given by Eq. (26) leads to

$$\varphi(t) = -\frac{1}{2}\,\mathrm{atan}\left(\frac{t}{t_R}\right). \tag{28}$$

The scaling $|A| \sim 1/\sqrt{w}$ expresses the fact that while the packet broadens the energy in the dissipation-free case under consideration should be conserved. The phase shift expressed by Eq. (28) is the analogous of the Gouy shift in optics and arises from the different phase speed of the various spectral components of the GAM packet. The factor 1/2 on the right-hand side of Eq. (28) arises because the GAM is a one-dimensional oscillation, see e.g. [63].

4.2 Paraxial WKB approach including damping

As explained in Sec. 3, the paraxial WKB equations maintain the same form (with the substitution $H \to H - i\Gamma$) if damping is included. Under the same assumptions of a uniform medium and quadratic dependence of the damping coefficient on the wavevector as before, the variables r_0 = const. and $k_0 = 0$ remain real even if the Hamiltonian is taken to be complex. The solutions derived above are therefore still valid (assuming Γ_{kk} = const.) and read, on splitting again real and imaginary part:

$$s(t) = \frac{s_0 X + \phi_0 Y}{X^2+Y^2}, \qquad \phi(t) = \frac{\phi_0 X - s_0 Y}{X^2+Y^2} \tag{29}$$

with

$$X \equiv 1 + (H_{kk}s_0 + \Gamma_{kk}\phi_0)\,t, \qquad Y \equiv (H_{kk}\phi_0 - \Gamma_{kk}s_0)\,t. \tag{30}$$

In the limit $\Gamma_{kk} \to 0$, these solutions reduce to Eqs. (20). It is interesting to notice that also in the opposite limit, $H_{kk} \to 0$, the width of the packet increases with time, i.e. undergoes a *dissipative* broadening. Eqs. (29-30) simplify in this case (for $s_0 = 0$) to

$$s(t) = 0, \qquad \phi(t) = \frac{\phi_0}{1+\Gamma_{kk}\phi_0 t}. \tag{31}$$

A k_r-dependent dissipation is seen to introduce the diffusive time scale

$$t_D = \frac{1}{\Gamma_{kk}\phi_0} \tag{32}$$

(where $t_D \geq 0$ if the damping increases with increasing k_r), so that the width of the packet evolves in time as

$$w(t) = w_0\sqrt{1+\frac{t}{t_D}}. \tag{33}$$

The fact that this is the solution of a one-dimensional diffusion equation for the width of a Gaussian distribution with initial condition $w(0) = w_0$ is not coincidental but is related to the fact that the imaginary part of the Hamiltonian introduces a diffusive term in the wave equation, see Appendix B and the discussion in Sec. 4.4. If both t_R and t_D are finite, the width of the packet $w = \sqrt{2/\phi}$ is, according to Eq. (29),

$$w(t) = w_0\sqrt{\frac{(1+t/t_D)^2 + t^2/t_R^2}{1+t/t_D}} \tag{34}$$

In the equation for $|A|$, both $H_{kk}s$ and $\Gamma_{kk}\phi$ contribute now to Re[div (H_k)]. The terms containing arc-tangent functions cancel in the integration of Eq. (10) and Eq. (27) generalizes in the case of damping to

$$\log \frac{|A(t)|}{|A_0|} = -\frac{1}{4} \log \left[\left(1 + \frac{t}{t_D} \right)^2 + \frac{t^2}{t_R^2} \right]. \tag{35}$$

In the limit $1/t_D \to 0$ (no damping), Eq. (27) is recovered. In the opposite limit, $1/t_R \to 0$ (negligible dispersion), the solution scales like

$$|A(t)| = \frac{w_0}{w(t)} \, |A_0| \tag{36}$$

with $w(t)$ given by Eq. (33), in agreement with the behaviour of a diffusive solution in dimension one. Obviously, the energy of the packet is not conserved in the damping process. It is interesting to note that while the first term in the damping coefficient (independent of k_r), see Eq. (4), leads to the usual exponential damping of the packet according to the *ansatz* $\psi \sim \exp[-\gamma t]$, the second term (proportional to k_r^2) does not contribute directly to the exponential damping, since $k_r = 0$ at the centre of the packet in the homogeneous case we are considering. This second term leads, on the other hand, to a finite value of t_D through the second derivative of the damping coefficient with respect to k_r, and thus to the "diffusive-like" damping expressed by Eq. (36).

As far as the phase is concerned, the terms contributing to Im[div (H_k)] are $\Gamma_{kk}s$ and $H_{kk}\phi$. In this case, the terms containing the logarithmic functions arising from the integration cancel and one obtains

$$\varphi(t) = -\frac{1}{2} \left[\operatorname{atan} \left(\frac{t}{t_R} + \frac{t_R t}{t_D^2} + \frac{t_R}{t_D} \right) - \operatorname{atan} \left(\frac{t_R}{t_D} \right) \right], \tag{37}$$

which is a generalization of the Gouy phase to the case of damped oscillations.

4.3 Wigner-function treatment

Also in the Wigner-function approach, the phase-space position of the centre of the packet is constant for $k_0 = 0$ because in this case $\Gamma_k = 0$ in Eqs. (13-14) (while $\Gamma_r = 0$ because of the medium uniformity). Thus, in the uniform case, also Eq. (15) simplify significantly to

$$\frac{\mathrm{d}}{\mathrm{d}t} \begin{pmatrix} G_{kk} & G_{kr} \\ G_{kr} & G_{rr} \end{pmatrix} = \begin{pmatrix} -2H_{kk}G_{kr} + \Gamma_{kk}\left(1 - G_{kr}^2\right) & -G_{rr}\left(H_{kk} + \Gamma_{kk}G_{kr}\right) \\ -G_{rr}\left(H_{kk} + \Gamma_{kk}G_{kr}\right) & -\Gamma_{kk}G_{rr}^2 \end{pmatrix}. \tag{38}$$

The solution for G_{rr} is immediate after separation of variables and reads

$$G_{rr}(t) = \frac{G_{rr,0}}{1 + \Gamma_{kk}G_{rr,0}t}. \tag{39}$$

The equation for G_{kr} can be also be solved by separation of variables:

$$\frac{\mathrm{d}G_{kr}}{H_{kk} + \Gamma_{kk}G_{kr}} = -\frac{G_{rr,0}\mathrm{d}t}{1 + \Gamma_{kk}G_{rr,0}t} \tag{40}$$

from which

$$\frac{H_{kk} + \Gamma_{kk}G_{kr}}{H_{kk} + \Gamma_{kk}G_{kr,0}} = \frac{1}{1 + \Gamma_{kk}G_{rr,0}t} \tag{41}$$

and finally

$$G_{kr}(t) = \frac{G_{kr,0} - H_{kk}G_{rr,0}t}{1 + \Gamma_{kk}G_{rr,0}t}. \tag{42}$$

A solution for G_{kk} is not required since, as noted before, two elements of the G matrix are sufficient to determine the two physics quantities of interest, namely $s(t)$ and $\phi(t)$.

Using the relations $G_{rr} = (s^2 + \phi^2)/\phi$ and $G_{kr} = -s/\phi$, see Eq. (12), one can easily check that the solutions of the paraxial WKB method (29) coincide with those of the Wigner approach. Eq. (16) for the amplitude of the Wigner function α reduces in the homogeneous case to

$$\frac{1}{\alpha}\frac{\mathrm{d}\alpha}{\mathrm{d}t} = -\frac{1}{2}\Gamma_{kk}G_{rr}, \tag{43}$$

with G_{rr} given by Eq. (39). After simple integration one has

$$\alpha(t) = \frac{\alpha_0}{\sqrt{1 + \Gamma_{kk}G_{rr,0}t}} = \frac{\alpha_0}{1 + t/t_D}, \tag{44}$$

where the last step follows from taking again $s_0 = 0$ as initial condition, so that $G_{rr,0} = \phi_0$. The wave energy density (proportional to $|\psi|^2$) is related to the Wigner function through an integral over wavevector space:

$$|\psi|^2 \propto \int W \mathrm{d}k_r = \alpha e^{-\phi(r-r_0)^2 - 2\gamma t} \int \exp\left[-(k_r - k_0 - s(r-r_0))^2/\phi\right] \mathrm{d}k_r, \tag{45}$$

where the last step comes from expressing the element of the matrix G in terms of s and ϕ using Eq. (12). The integral over a shifted Maxwellian yields simply $\sqrt{\pi\phi}$. After substitution of ϕ from Eq. (29), again with $s_0 = 0$, we find

$$|\psi|^2 \propto \frac{e^{-\phi(r-r_0)^2 - 2\gamma t}}{\sqrt{(1 + t/t_D)^2 + t^2/t_R^2}}, \tag{46}$$

consistently with Eq. (35).

4.4 Physical interpretation of dissipative broadening

In Sec. 4.2 it was observed that a non trivial evolution (of diffusive kind) of the width of the packet can be induced by a finite second-order derivative of the damping coefficient with respect to k_r, i.e. $\Gamma_{kk} \neq 0$. Physically, a damping coefficient of the form $\gamma = f + gk_r^2$ with $g > 0$ implies that higher components of the Gaussian k_r-spectrum constituting the packet are dissipated more strongly than smaller wavevectors. This results in a shrinking of the k_r-spectrum and hence in a broadening of the packet in real space. To simplify the discussion we can take the limit $H_{kk} \to 0$. In the case of GAMs, the limit of negligible (real) dispersion can be achieved when α_1 in Eq. (1) is close to zero.

One can model this situation by considering that a wave packet of initial width w_0 exhibits a spectral width $2/w_0$. Applying the selective damping of the higher spectral components and transforming back to real space one finds

$$\psi \sim \frac{1}{2\pi}\int e^{ik_r x} e^{-w_0^2 k_r^2/4} e^{-(f+gk_r^2)t} \mathrm{d}k_r = \frac{e^{-ft}}{\sqrt{\pi}} \frac{e^{-x^2/(w_0^2+4gt)}}{\sqrt{w_0^2 + 4gt}}, \tag{47}$$

where $x = r - r_0$. This shows that the maximum of the wave packet is damped exponentially by the term including f, while its width increases according to Eq. (33), since clearly $\Gamma_{kk} = 2g$ and $1/t_D = \Gamma_{kk}\phi_0 = 4g/w_0^2$. As mentioned above, these analogies with a diffusion process are not really surprising given the fact that Γ_{kk} introduces a diffusion term in the equation for W, Eq. (B.18) or, correspondingly, that $\exp(-gk_r^2 t)$ is the Fourier transform of the heat kernel.

5 Inhomogeneous plasma, no damping

If the plasma parameters, most importantly the temperature, vary with radius, the wave vector evolves from its initial value $k_r = 0$ at the centre of the packet. If the radial variation

of the plasma parameters can be approximated as linear, then k_r increases linearly with time and the position of the packet scales quadratically with time ("GAM acceleration" [36]). Analytic solutions for the packet evolution can be obtained in this limit of linear radial dependence of the dispersion relation. In this section, the solution of the paraxial WKB equations presented in [37] is summarized and shown to coincide again with the corresponding solution for the Wigner function.

The GAM frequency ω_0 is assumed here to exhibit a linear radial profile

$$\omega_0 \to \omega_0 \left(1 - \frac{r - r_0}{2L_T}\right), \tag{48}$$

which results from a linear variation of the thermal ion speed (the factor 1/2 appearing in the last term has been introduced for consistency with a Taylor expansion of the temperature profile, assumed to vary as $1-(r-r_0)/L_T$). For the imaginary part of the dispersion function, the approximation of "weak variation" of the dispersion relation across the width of the packet is more critical, since the (Landau) damping varies exponentially with ω_0, as discussed in Sec. 2. Damping will be ignored in the remainder of this section. Experimentally, GAMs are known to appear also in form of eigenmodes, which oscillate with constant frequency across a finite radial extent [64, 65] also in non-uniform equilibria. This feature is known from theory [5, 66, 67] and has been reproduced also numerically [68, 69]. Here, we suppose the GAM behaves as a continuum [32], i.e. it oscillates at the local (radially varying) frequency given by Eq. (1) with Eq. (48). In the applications of the paraxial theories discussed in [36, 37], however, the parameters were selected in such a way that the packet retained largely its structure in the time interval under investigation.

5.1 Paraxial WKB treatment

In the case of linear variation of the Hamiltonian with r, we have $H_{rr} = 0$ and Eq. (8) reduces to a Bernoulli equation which can be solved for its inverse as in the homogeneous case. Setting $u = 1/\overline{s}$ Eq. (8) becomes

$$\frac{\mathrm{d}u}{\mathrm{d}t} - 2H_{kr}u = H_{kk} \tag{49}$$

which has the solution

$$u(t) = e^{-F(t)} \left(u_0 + \int_0^t H_{kk}(t')e^{F(t')}\mathrm{d}t'\right), \tag{50}$$

with

$$F(x) = -2\int_0^x H_{kr}(y)\mathrm{d}y. \tag{51}$$

In the homogeneous limit considered in the previous section, $F \equiv 0$ and Eq.(50) reproduces Eq. (18).

The solution of the ray equations for the inhomogeneous case has been given in [36]. The equation for the wave vector

$$\frac{\mathrm{d}k_r}{1 + \alpha_1 k_r^2 \rho_i^2/2} = \frac{\omega_0}{2L_T}\mathrm{d}t \tag{52}$$

has the solution

$$k_r = \begin{cases} (\alpha_1 > 0) & \tan\left(\sqrt{\alpha_1\rho_i^2/2}\ \omega_0 t/2L_T\right)/\sqrt{\alpha_1\rho_i^2/2} \\ (\alpha_1 < 0) & \tanh\left(\sqrt{|\alpha_1|\rho_i^2/2}\ \omega_0 t/2L_T\right)/\sqrt{|\alpha_1|\rho_i^2/2} \end{cases}. \tag{53}$$

For small values of the argument (which amounts to the condition $\rho_i/L_T \ll 1$ for times of the order of some inverse transit frequencies) one has

$$k_r = \frac{\omega_0 t}{2L_T}. \tag{54}$$

Eq. (54) recovers explicitly the corresponding limiting case of Eq. (A5) of [36]. The equation for the position of the centre of the wave packet

$$\frac{\mathrm{d}r}{1-(r-r_0)/2L_T} = \alpha_1 \rho_i^2 \omega_0 k_r \mathrm{d}t \tag{55}$$

has the solution

$$\frac{r-r_0}{2L_T} = 1 - \exp\left[-\alpha_1 \rho_i^2 \frac{\omega_0^2}{8L_T^2} t^2\right]. \tag{56}$$

Taking again the limit for small values of the argument of the exponential function one has

$$\frac{r-r_0}{L_T} \simeq \alpha_1 \rho_i^2 \frac{\omega_0^2}{4L_T^2} t^2, \tag{57}$$

which coincides with Eq. (A7) of [36].

Using Eqs. (54,57) the integrals in the paraxial solution (50) can be calculated explicitly. This leads to the solution

$$u(t) = u_0 e^{-Ct^2} - \alpha_1 \rho_i^2 \omega_0^2 t + \frac{3}{2}\alpha_1 \rho_i^2 \omega_0^2 \sqrt{\frac{\pi}{C}} e^{-Ct^2} \,\mathrm{erfi}\left(\sqrt{C}t\right), \tag{58}$$

with $C \equiv \alpha_1 \rho_i^2 \omega_0^2 / 2L_T^2$. Performing again a small-argument expansion, using $\mathrm{erfi}(x) \simeq 2x/\sqrt{\pi}$, Eq. (58) becomes to lowest order in t

$$u(t) = u_0 + \alpha_1 \rho_i^2 \omega_0 t, \tag{59}$$

which coincides with the solution found in the homogeneous limit, Eq. (18).

5.2 Wigner-function treatment

In the Wigner approach, the equations for the centre of the packet are the same as in the paraxial WKB theory if damping is neglected. Recalling that $H_{rr} = 0$, Eq. (15) takes the form

$$\frac{\mathrm{d}G}{\mathrm{d}t} = \begin{pmatrix} 2H_{kr}G_{kk} - 2H_{kk}G_{kr} & -H_{kk}G_{rr} \\ -H_{kk}G_{rr} & -2H_{kr}G_{rr} \end{pmatrix} \tag{60}$$

The equation for G_{rr} can be solved immediately and gives

$$G_{rr}(t) = G_{rr,0} \exp\left[-2\int_0^t H_{kr}(t')\mathrm{d}t'\right] = G_{rr,0} e^{F(t)}, \tag{61}$$

with $F(t)$ defined in Eq. (51). The solution for G_{kr} is also straightforward,

$$G_{kr}(t) = G_{kr,0} - G_{rr,0} \int_0^t H_{kk}(t') e^{F(t')} \mathrm{d}t'. \tag{62}$$

These solutions can be compared with those of the paraxial WKB method, Eq. (50). Since $u = 1/\overline{s} = (s - i\phi)/(s^2 + \phi^2)$, one has from Eq. (12)

$$\frac{1}{G_{rr}} = \frac{\phi}{s^2+\phi^2} = -\mathrm{Im}(u) \qquad \frac{G_{kr}}{G_{rr}} = -\frac{s}{s^2+\phi^2} = -\mathrm{Re}(u). \tag{63}$$

Substituting the solutions for G_{rr}, Eq. (61), G_{kr}, Eq. (62), and u, Eq. (50), in the previous equation, one can verify that the solutions obtained with both approaches are indeed identical.

6 Gyrokinetic simulation of GAM packets

The analytic results presented in the previous sections are compared here with numerical simulations of the evolution of a Gaussian GAM packet obtained with the gyrokinetic particle-in-cell code ORB5. The equations solved by the code and in particular their application to the GAM problem are detailed elsewhere [36, 37] and are not reported here. It is just remarked that in these simulations the gyrokinetic Vlasov-Poisson problem is solved in the linear and electrostatic limit across the whole radial domain of a tokamak with circular concentric flux surfaces. Unless specified differently, density, temperature and safety-factor profiles are taken to be flat. The electron-to-ion temperature ratio $\tau_e = T_e/T_i$ and the value of the safety factor q are employed as the main handle on the dispersive and dissipative properties of the plasma with respect to GAMs. The electron response is treated as adiabatic. A Gaussian electric-field perturbation in radial direction, centred around $r_0/a = 0.5$ with width $w/a = 0.04$, is initialized through a corresponding perturbation of the ion density. Further parameters are the major radius $R_0 = 1.3$ m, minor radius $a = 0.13$ m, magnetic field on axis $B_0 = 1.9$ T and $L_r = 2a/\rho_s = 320$ (where ρ_s is the sound Larmor radius).

As a first example, a damping-free case as those discussed in detail in [37] is selected by taking $\tau_e = 18$ and $q = 5$. The first plot of Fig. 1 shows the absolute value of the radial electric field (normalized to its peak value at $t = 0$) as a function of the time t and of the normalized radial coordinate r/a. In this representation, the analogy between the behaviour of the packet and the propagation of a wave beam in optics (in which case the time coordinate would be substituted by a space coordinate) becomes particularly evident. The cyan and red curves overlaid to the numerical results have been obtained by following the points corresponding to a given level ($1/e$ and $1/e^2$ respectively) of the *initial* maximum of the electric-field amplitude at $t = 0$, slightly corrected as explained below. It is noted that the width of the packet at time t, as obtained directly from Eq. (22), describes the $1/e$-level of the GAM electric field with respect to the maximum of the envelope calculated at the same time t. A curve connecting the points corresponding to a given fraction C of the initial amplitude maximum can be obtained by observing that paraxial field ansatz, Eq. (B.2), and Eq. (35) imply

$$\frac{|\psi|}{|\psi_0|} = C \Rightarrow -\frac{1}{4}\log\left[\left(1+\frac{t}{t_D}\right)^2 + \frac{t^2}{t_R^2}\right] - \frac{(r-r_0)^2}{w^2(t)} = \log C \tag{64}$$

from which

$$r - r_0 = \mp w(t)\sqrt{-\log C - \frac{1}{4}\log\left[\left(1+\frac{t}{t_D}\right)^2 + \frac{t^2}{t_R^2}\right]} \tag{65}$$

with $w(t)$ from Eq. (34) and $C = 1/e$ or $C = 1/e^2$ for the cyan and red curves in Fig. 1, respectively. The usefulness of this equation is simply that it is designed to follow the edge of the contours with the same colour, while the width w would deviate from it with decreasing amplitude $|A|$ (which is the meaning of the correction in the second term of the previous equation).

The agreement between the numerical simulation and the analytic solutions presented in the previous sections is particularly clear from the bottom plot in Fig. 1, which represents the time evolution of the GAM electric field at the centre of the packet, $r = r_0$. As shown in [37], the inclusion of the Gouy phase shift leads to an almost perfect superposition of analytic and numerical solution. It has to be remarked, however, that in the numerical simulations a short transient phase at the beginning of the simulation is often observed, which leads to a comparatively strong drop of the amplitude during the first two or three oscillations, after which the time evolution of the envelope becomes smooth. In the plots presented in this section, therefore, the initial amplitude of the analytic solution has been chosen as to match the numerical value after this transient phase. Furthermore,

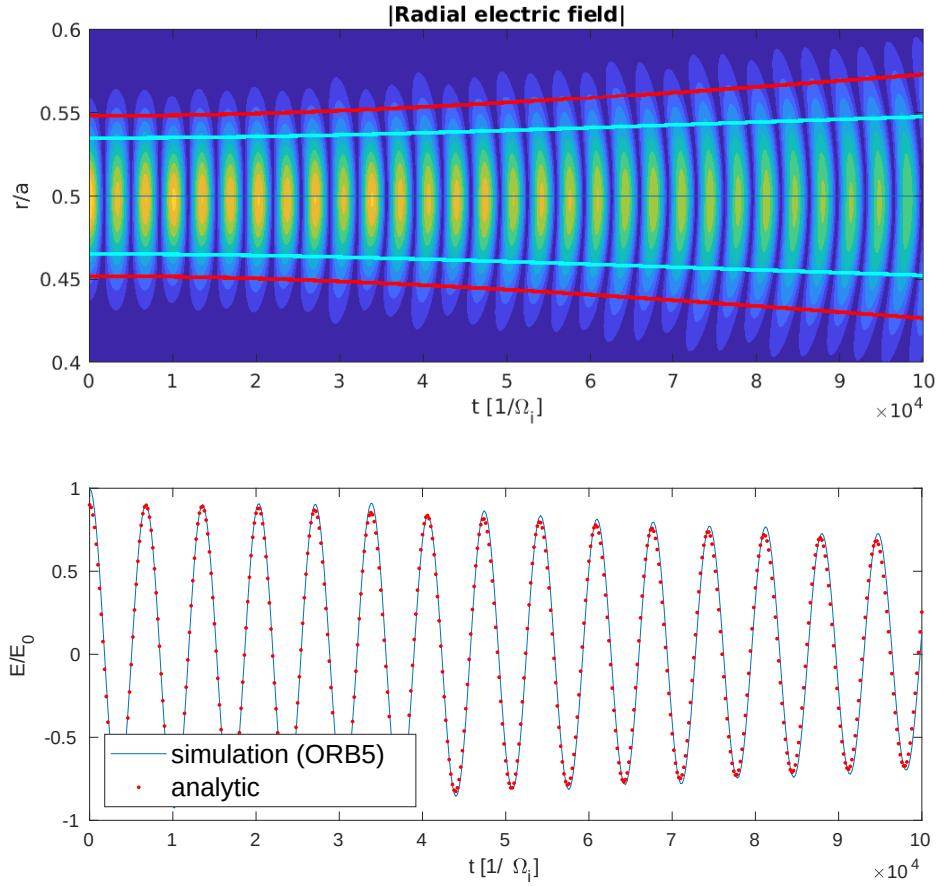

Figure 1: *Time evolution of the absolute value of the radial electric field for electron-to-ion temperature ratio $\tau_e = 18$ and safety factor $q = 5$. Overlaid in the upper plot ($t - r$ plane) are the curves at level $1/e$ (cyan) and $1/e^2$ (red) of the initial maximum. In the lower plot the value of the electric field at $r/a = 0.5$ as obtained in the simulations is compared to the analytic predictions derived in Sec. 4.*

as observed in previous work (see Fig. 16 of [36]), the value of parameter α_1 governing the strength of the dispersion can deviate from the value inferred e.g. through the displacement of the centre of the packet with time as inferred from its "ray" trajectory. The agreement between simulations and theory improves with increasing q, consistently with the approximations performed in the theoretical derivation of α_1.

A stronger impact of the damping on the GAM evolution is achieved through a reduction of τ_e or q, as in both cases the Landau damping on the ions is moved towards the thermal bulk. As shown in Fig. 2, for the parameters chosen in our simulations the "diffusive" time scale due to stronger absorption of higher k_r can compete or overcome the dispersive ("Rayleigh") time scale only for $q = 2$ and relatively low values of τ_e. At values of $\tau_e \lesssim 3$, the ordering under which the damping rate shown in Eq. (4) has been derived starts to break down, as the ion Larmor radius is increased so that $k_r \rho_i$ can be equal or exceed $1/q^2$ for typical spectral components $k_r \sim 2/w_0$. For the same reason, the damping rate considered here might become inaccurate at higher values of q. These issues are discussed later in this section. Different or more accurate models may be able to treat these regions of parameter space better than those considered here. It is stressed that the focus of this paper is on the derivation and basic validation of the formalism described in the previous sections, for which simpler formulas are better suited and allow

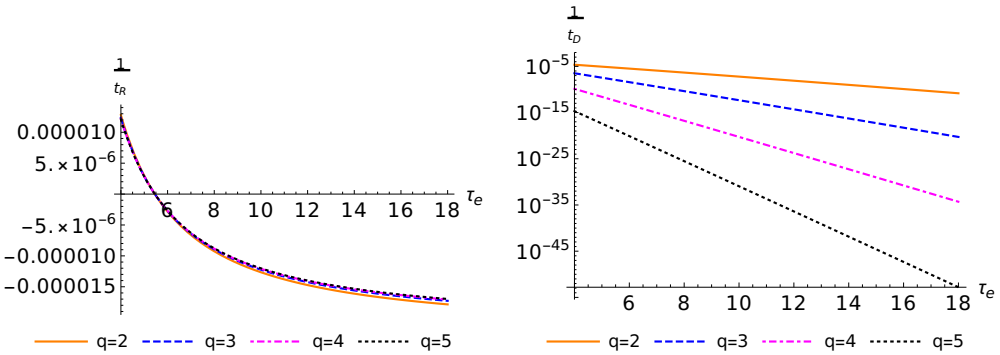

Figure 2: *Inverse Rayleigh time (left) and inverse diffusive time (right) in units of* Ω_i *as a function of* τ_e *for different values* q*.*

a straightforward derivation. An analysis of the applicability of the present formalism to the case of more complicated Hamiltonians (i.e. dispersion relations) is left for future work.

Fig. 3 shows the absolute value of the GAM electric field as a function of time and radius for $\tau_e = 7$ and $q = 5$ (upper plot) and $q = 3$ (lower plot). Since for this value of τ_e the factor α_1 ruling the "dispersiveness" of the plasma is close to 0, the dispersive broadening is significantly smaller than in Fig. 1. The main difference which can be appreciated between the two values of q considered in Fig. 3 is the flattening of the "wave fronts" (or, in other words, the fact that the GAM oscillation occurs simultaneously over the whole radial extent of the packet) in the case $q = 3$ as compared to $q = 5$. This is in agreement with the behaviour described by Eq. (29) in the limit of vanishing dispersion, Eq. (31). On the other hand, according to Fig. 2 this effect should still not be visible, given the fact that for the considered values $1/t_D$ is still smaller than $1/t_R$. This seems to suggest that Eq. (4) does not reproduce quantitatively the damping rate found in the simulations for these parameters, as discussed above.

The results of a simulation in which the diffusive time scale is shorter than the dispersive time scale (this is obtained by choosing $\tau_e = 4$ and $q = 2$) are finally reported in Fig. 4. Notice that α_1 is positive for this value of τ_e, while it is negative for the case $\tau_e = 18$ reported in Fig. 1. Correspondingly, the "phase fronts" have a different shape in both figures, reflecting the fact that the edges of the packet oscillate faster than the centre for $\alpha_1 < 0$ and slower than the centre for $\alpha_1 > 0$.

For $q = 2$ and $\tau_e = 4$, the damping rate (4) is expected to describe correctly the damping process. Due to the strong decrease of GAM energy, the cyan lines connecting the points which correspond to an electric field amplitude smaller by a factor $1/e$ with respect to the initial maximum, drawn according to Eq. (65), close on themselves before half of the simulation time is elapsed. The time evolution of the electric field maximum according to the analytic formulas derived in the previous section is seen to accurately reproduce the results of the simulation also in this strongly-damped regime.

7 Summary and final remarks

Two different sets of paraxial equations, which include damping effects without any ordering assumption on their magnitude, have been employed for the description of damped geodesic acoustic oscillations. Although derived in the context of non-Hermitian quantum systems, this approach turns out to be applicable also in other systems because of the formal equivalence between the Schrödinger equation and the paraxial wave equation. In the case of homogeneous plasmas, simple analytic solutions can be obtained for the time evolution of the GAM electric field, which highlight in particular the effect of selective

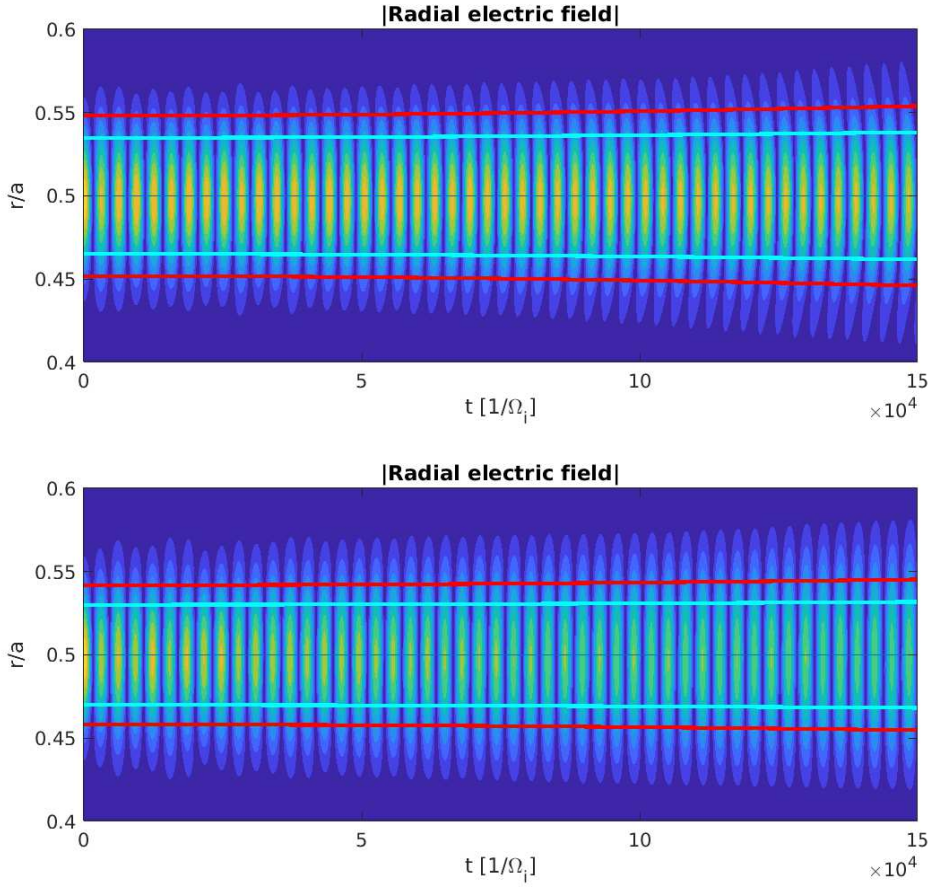

Figure 3: *Absolute value of the GAM electric field as a function of time and radius for* $\tau_e = 7$ *and* $q = 5$ *(upper plot) and* $q = 3$ *(lower plot). Cyan and red curves are like in Fig. 1.*

dissipation of higher wavenumbers on the shape of a GAM packet. The predictions of the analytic theory are confirmed by linear gyrokinetic simulations performed with the code ORB5.

As a technical remark, it is noted that the equivalence between the Wigner-function approach and the complex pWKB method has been proved in [54] only for the case of Hamiltonians which are quadratic in the position and momentum variables (this includes linear terms). In particular, in this case a projection of the (in general complex-valued) pWKB solution to real space is provided, which can be shown to lead to the same results as for the Wigner-function approach. How far this equivalence can be extended to more general Hamiltonians is an open issue. It is stressed, however, that the Wigner-function approach can be employed for general Hamiltonians, as long as the wave equation can be cast in the form of a paraxial ("Schrödinger") equation, cf. App. B. Moreover, for all the cases considered in this paper, the "ray trajectories" determined through Eqs. (7) [cf. also Eqs. (13-14)] do not leave the real space because the terms proportional to the first-order derivatives of the imaginary part of the Hamiltonian vanish. This is either due to the fact that the wave vector k_r at the centre of the packet is identically zero (homogeneous case, Sec. 4.2) or that damping has been excluded (inhomogeneous case, Sec. 5), but the theory is not limited to such cases. The investigation of complex ray trajectories is left for future work.

As far as our understanding of geodesic acoustic modes is concerned, the results pre-

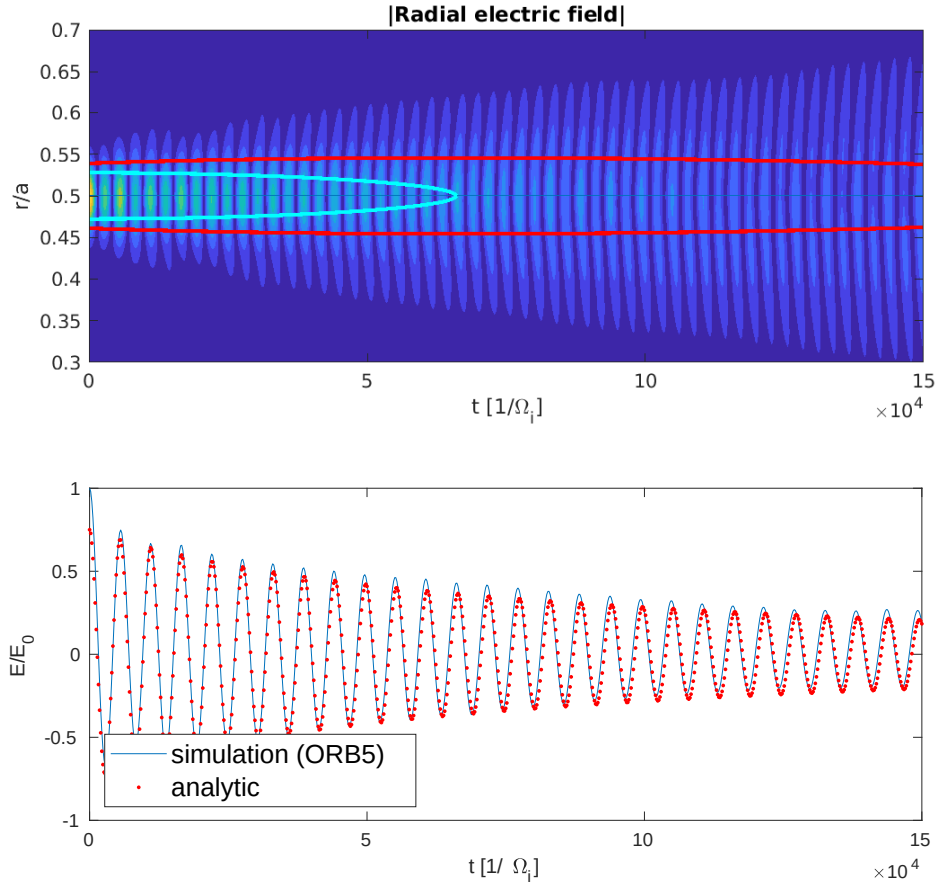

Figure 4: *Time evolution of the absolute value of the radial electric field as in Fig. 1, here for* $\tau_e = 4$ *and* $q = 2$.

sented in this paper complement those discussed in [36, 37] and demonstrate the accuracy of the quasi-optical techniques in predicting the linear evolution of GAM packets. This implies that the parameter dependence of their linear dynamics can be extracted from analytic solutions without resorting to computationally expensive numerical simulations. Apart from this intrinsic relevance for the physics of GAMs, the present analysis is intended as an exploratory investigation of the potentialities of the complex-Hamiltonian approach, whose range of applicability has not been studied here beyond the simple scalar, one-dimensional case of the GAM radial electric field with quadratic Hamiltonian. It is likely that the same approach can be applied to more complicated situations. An interesting example could be represented by the paraxial description of tokamak eigenmodes proposed in [50], see also the introductory remarks in Sec. 1. Possible analogies with or extensions to other treatments involving the Wigner function for both low-frequency (e.g. [70] and references therein), and high-frequency waves (e.g. [59, 71] and references therein) shall be considered as well. More generally, a topic which was not addressed in this paper is the possibility of extending the treatment presented here towards nonlinear applications. In this sense, it should be mentioned that methods for describing the dynamics of (paraxial) wave packets are widely employed in several contexts beyond plasma physics, most notably in optics (indeed the approach employed in this paper was already applied to the propagation of beams in the presence of gain or loss [72]) and more specifically in nonlinear optics, where spatial optical solitons or temporal solitons in optical fibers emerge as a solution of a nonlinear Schrödinger equation [73, 74]. As far as a Wigner-Moyal ap-

proach is concerned, it was observed almost two decades ago in both physical [75] and mathematical [76] literature that a nonlinear Schrödinger equation can be converted into a Vlasov-like equation for the relevant Wigner function, which leads to striking analogies with typical plasma-physics phenomena, like optical bump-on-tail instabilities [77]. But also in the frame of fusion applications, it has been shown [78, 79, 80, 81] that the evolution of the radial envelope of an Alfvénic wave packet interacting with a population of energetic particles can be expressed as a Schrödinger equation with integro-differential nonlinear terms, which in the case of energetic-particle modes can be cast into a special form of the complex Ginzburg-Landau equation [82, 83]. Extensions of the present work in this direction will be explored in the future.

Acknowledgments

This work has been carried out within the framework of the EUROfusion Consortium and has received funding from the Euratom research and training programme 2014-2018 and 2019-2020 under grant agreement No 633053. The views and opinions expressed herein do not necessarily reflect those of the European Commission. We acknowledge the support from Enabling Research Project ENR-MFE19.MPG-01.

Enlightening discussions with E.-M. Graefe are gratefully acknowledged. E. P. would like to thank T. Hayward-Schneider for his help with the setup of the ORB5 simulations.

The data that support the findings of this study are available from the corresponding author upon reasonable request.

A Basic definitions

The Weyl symbol maps the kernel $\mathcal{A}(x,x')$ of an integral operator $\hat{A}[f] = \int \mathcal{A}(x,x')f(x')\mathrm{d}x'$ into phase space according to

$$A(x,k) = \int e^{-iks}\mathcal{A}\left(x+\frac{s}{2}, x-\frac{s}{2}\right)\mathrm{d}s \tag{A.1}$$

(Weyl symbols are denoted by capital letters). Following [84], we define the "common" or "standard" (unsymmetrized) symbol (denoted by a lowercase letter)

$$a(x,k) = \int e^{-iks}\mathcal{A}\left(x, x-s\right)\mathrm{d}s. \tag{A.2}$$

These symbols are related through

$$A(x,k) = e^{(i/2)\partial_k\partial_x}a(x,k) \sim \sum_{n=0}^{\infty}\frac{1}{n!}\left(\frac{i}{2}\right)^n\left(\frac{\partial}{\partial k}\frac{\partial}{\partial x}\right)^n a(x,k). \tag{A.3}$$

In general, the series is asymptotically convergent only, each term scaling with $1/(kL)^n$ for large k. The Weyl symbol of the composition of two operators $\hat{A}$ and $\hat{B}$ is given by the so-called Weyl-Moyal product

$$C(x,k) = A(x,k)\star B(x,k) \sim A(x,k)e^{(i/2)[\overleftarrow{\partial_x}\overrightarrow{\partial_k}-\overleftarrow{\partial_k}\overrightarrow{\partial_x}]}B(x,k), \tag{A.4}$$

where the arrows denote if the differentiation acts on the symbol on the left or on the right and the exponential is defined as before in terms of the corresponding (asymptotically converging) series.

B Derivation of the paraxial equations

We assume that the GAM dynamics can be described by an equation of the form

$$i\frac{\partial\psi}{\partial t} = \mathcal{F}\psi - \frac{1}{2}\frac{\partial}{\partial r}\left[\mathcal{G}\frac{\partial\psi}{\partial r}\right] \tag{B.1}$$

which is an equation of the form $i\partial_t\psi = \widehat{\overline{H}}\psi$, with the Hamiltonian operator $\widehat{\overline{H}}$ defined by the right-hand side of the previous equation. The complex functions $\mathcal{F}$ and $\mathcal{G}$ reflect the dispersive (real part) and dissipative (imaginary part) properties of the GAM and can be read off directly from Eqs. (1,4,5).

The paraxial WKB equations follow from direct substitution of the paraxial *ansatz* for the field (with $\overline{\omega} = \omega - i\gamma$),

$$\psi(t,r) = A(t)e^{i[k_0(t)(r-r_0(t))+\frac{1}{2}\overline{s}(t)(r-r_0(t))^2-\overline{\omega}t]} \tag{B.2}$$

into Eq. (B.1) and separation of different powers of $r - r_0$. In this process, $\mathcal{F}$ and $\mathcal{G}$ are expanded to second order around r_0 and $\partial\mathcal{G}/\partial r$ to first order. The terms proportional to $r - r_0$ give

$$-\frac{\mathrm{d}k_0}{\mathrm{d}t} + \overline{s}\frac{\mathrm{d}r_0}{\mathrm{d}t} = \frac{\partial\mathcal{F}}{\partial r} + \frac{1}{2}\frac{\partial\mathcal{G}}{\partial r}k_0^2 + \mathcal{G}k_0\overline{s}, \tag{B.3}$$

while the terms proportional to $(r - r_0)^2$ lead to an equation for $\overline{s}$:

$$-\frac{\mathrm{d}\overline{s}}{\mathrm{d}t} = \frac{\partial^2\mathcal{F}}{\partial r^2} + \frac{1}{2}\frac{\partial^2\mathcal{G}}{\partial r^2}k_0^2 + 2\frac{\partial\mathcal{G}}{\partial r}k_0\overline{s} + \mathcal{G}\overline{s}^2. \tag{B.4}$$

The remaining terms give the transport equation for the amplitude:

$$\frac{1}{A}\frac{\mathrm{d}A}{\mathrm{d}t} = i\left[k_0\frac{\mathrm{d}r_0}{\mathrm{d}t} + \overline{\omega} - \left(\mathcal{F} + \frac{1}{2}\mathcal{G}k_0^2\right)\right] - \frac{1}{2}\left(\frac{\partial\mathcal{G}}{\partial r}k_0 + \mathcal{G}\overline{s}\right). \tag{B.5}$$

We introduce the complex Hamiltonian $\overline{H}$ defined as

$$\overline{H} = \mathcal{F}(r) + \frac{1}{2}\mathcal{G}(r)k_r^2, \tag{B.6}$$

and choose $\overline{\omega}$ so that $\overline{H} = \overline{\omega}$ on the central trajectory, see Eq. (5). Calculating explicitly the relevant derivatives of $\overline{H}$, it is straightforward to recast the previous equations in the form:

$$\frac{\mathrm{d}r_0}{\mathrm{d}t} = \overline{H}_k \qquad \frac{\mathrm{d}k_0}{\mathrm{d}t} = -\overline{H}_r \tag{B.7}$$

$$\frac{\mathrm{d}\overline{s}}{\mathrm{d}t} = -\overline{H}_{rr} - 2\overline{H}_{kr}\overline{s} - \overline{H}_{kk}\overline{s}^2 \tag{B.8}$$

$$\frac{\mathrm{d}A}{\mathrm{d}t} = A\left[ik_0\frac{\mathrm{d}r_0}{\mathrm{d}t} - \frac{1}{2}\mathrm{div}\,\left(\overline{H}_k\right)\right], \tag{B.9}$$

where the last term in Eq. (B.9) represents the divergence of the group velocity,

$$\mathrm{div}\,\left(\overline{H}_k\right) = \overline{H}_{kr} + \overline{H}_{kk}\overline{s}. \tag{B.10}$$

It should be remarked at this point that, contrary to the usual derivation of WKB equations for plasma waves, see e.g. [85], no ordering assumption has been made on the magnitude of the damping rate, i.e. on the imaginary part of $\overline{\omega}$. As a consequence [86], dissipation does not appear explicitly in Eq. (B.9). Apart from this difference, Eqs. (B.7-B.9) are the equations of the paraxial WKB method as derived e.g. by Pereverzev [44], specialized to the case of a scalar field and a one-dimensional system. For the sake of completeness we note that, in principle, the trajectory of the centre of the packet as described by Eq. (B.7) becomes complex (although this case is not considered in the present paper), and the functions $\mathcal{F}$ and $\mathcal{G}$ should be required to be analytic. Analogous equations have been derived for quantum-mechanical applications in the past, see e.g. [87, 88]. In this paper, a set of equations for the Wigner transform of the field given by Eq. (B.2) is also applied to the determination of the dynamics of a GAM packet. The derivation of these equations is reported in [53] and summarized below, slightly adapted to the classical situation under consideration.

As for the density matrix in quantum mechanics, we can introduce an operator $\hat{W} = \psi\psi^\dagger$, whose action on a test function f is

$$\hat{W}f = \int \psi(x)\psi^\dagger(x')f(x')\mathrm{d}x'. \tag{B.11}$$

Multiplying the equation $i\partial_t\psi = \widehat{\overline{H}}\psi$ by $\psi^\dagger$ and its adjoint by ψ, and adding them together one can derive

$$i\frac{\partial\hat{W}}{\partial t} = \widehat{\overline{H}}\hat{W} - \hat{W}\widehat{\overline{H}}^\dagger. \tag{B.12}$$

Introducing $\widehat{H} = (\widehat{\overline{H}} + \widehat{\overline{H}}^\dagger)/2$ and $\widehat{\Gamma} = i(\widehat{\overline{H}} - \widehat{\overline{H}}^\dagger)/2$, the previous equation becomes the Liouville-von-Neumann equation for $\hat{W}$, generalized to the case of a non-Hermitian Hamiltonian:

$$i\frac{\partial\hat{W}}{\partial t} = [\widehat{H}, \hat{W}] - i[\widehat{\Gamma}, \hat{W}]_+, \tag{B.13}$$

where $[\cdot,\cdot]_+$ denotes the anticommutator. This equation is translated into an equation involving the Weyl symbols H and Γ of the Hamiltonian, and the Wigner function W (Weyl symbol of the spectral operator), according to the Weyl-Moyal product introduced in Eq. (A.4). For the terms involving H, the commutator in Eq. (B.13) implies that only odd powers in the expansion of the exponential operator in Eq. (A.4) contribute to the Weyl-Moyal product. Expansion to second order gives then

$$H \star W - W \star H = i\left(\frac{\partial H}{\partial r}\frac{\partial W}{\partial k} - \frac{\partial H}{\partial k}\frac{\partial W}{\partial r}\right) + \dots. \tag{B.14}$$

The left-hand side of Eq. (B.14) exhibits a Poisson-bracket structure multiplied by the imaginary unit and leads to the classical Liouville equation (in the limit $\Gamma \to 0$). On the contrary, in the expansion of $\Gamma \star W + W \star \Gamma$ only even powers contribute to the product in Eq. (A.4). To second order this yields

$$\Gamma \star W + W \star \Gamma \sim 2\Gamma W - \frac{1}{4}\left(\frac{\partial^2\Gamma}{\partial r^2}\frac{\partial^2 W}{\partial k^2} - 2\frac{\partial^2\Gamma}{\partial k\partial r}\frac{\partial^2 W}{\partial k\partial r} + \frac{\partial^2\Gamma}{\partial k^2}\frac{\partial^2 W}{\partial r^2}\right) + \dots. \tag{B.15}$$

The previous equations can be written in compact form switching to the phase-space variable $z = (k_r, r)$ and introducing the matrix Ω defined as

$$\Omega = \begin{pmatrix} 0 & -1 \\ 1 & 0 \end{pmatrix}. \tag{B.16}$$

In terms of Ω, Eq. (A.4) becomes

$$A(r,k_r) \star B(r,k_r) \sim A(r,k_r)e^{(i/2)\overleftarrow{\nabla}\Omega\overrightarrow{\nabla}}B(r,k_r), \tag{B.17}$$

where ∇ denotes differentiation with respect to z. The evolution equation for the Wigner function W can be written as

$$\frac{\partial W}{\partial t} = \left[\frac{1}{4}\Delta_\Gamma + \nabla H\Omega\nabla - 2\Gamma\right]W, \tag{B.18}$$

where $\Delta_\Gamma = \nabla\Gamma''_\Omega\nabla$, with $\Gamma''_\Omega = \Omega^{\mathrm{t}}\Gamma''\Omega$ and Γ'' is the matrix of second derivatives of Γ. The imaginary part of the Hamiltonian Γ leads to the appearance of the diffusion term in Eq. (B.18). We truncate the right-hand side of Eq. (B.18) retaining the terms written explicitly on its right-hand side and look for a solution in terms of a Gaussian *ansatz* for the Wigner function,

$$W(t,z) = \alpha(t)e^{-(z-z_0(t))\cdot G(t)(z-z_0(t))-2\gamma t}, \tag{B.19}$$

into Eq. (B.18) and splitting the different powers of $z - z_0$ leads to

$$\frac{\mathrm{d}z_0}{\mathrm{d}t} = \Omega \nabla H - G^{-1} \nabla \Gamma \tag{B.20}$$

from the terms linear in $z - z_0$,

$$\frac{\mathrm{d}G}{\mathrm{d}t} = H'' \Omega G - G \Omega H'' + \Gamma'' - G \Gamma''_\Omega G \tag{B.21}$$

from the terms quadratic in $z - z_0$ and

$$\frac{1}{\alpha} \frac{\mathrm{d}\alpha}{\mathrm{d}t} = -\frac{1}{2} \mathrm{Tr}[\Gamma''_\Omega G] \tag{B.22}$$

from the remaining terms. Use has been made of the fact that $\Omega^{\mathrm{t}} = -\Omega$ and the symmetry of the matrix G has been enforced by the substitution $G \to (G + G^{\mathrm{t}})/2$ in Eq. (B.21). Explicit evaluation of the matrix multiplications in the previous equations leads to Eqs. (13-16).

C Relation between $\overline{s}$ and G

The Wigner function associated to a field

$$\psi = A e^{ik_0 x + (i/2)\overline{s} x^2}, \tag{C.1}$$

with $x = r - r_0$ and $\overline{s} = S + i\Phi$ can be readily calculated according to the definition

$$\begin{aligned} W &= \int e^{ik_r s} \psi \left(x + \frac{s}{2}\right) \psi^* \left(x - \frac{s}{2}\right) \mathrm{d}s \\ &= |A|^2 e^{-\Phi x^2} \int e^{i(-k + Sx)s - \Phi s^2/4} \mathrm{d}s \\ &= \frac{2\,|A|^2}{\sqrt{\Phi/\pi}} e^{-[(\Phi + S^2/\Phi)x^2 - 2(S/\Phi)kx + k^2/\Phi]} \end{aligned} \tag{C.2}$$

with $k = k_r - k_0$. Eq. (12) for the elements of the G matrix follow directly from the previous expression.

References

[1] N. Winsor, J. L. Johnson, and J. M. Dawson *Physics of Fluids*, vol. 11, p. 2448, 1968.

[2] K. Hallatschek and D. Biskamp *Physical Review Letters*, vol. 86, p. 1223, 2001.

[3] K. Itoh, K. Hallatschek, and S.-I. Itoh *Plasma Physics and Controlled Fusion*, vol. 47, p. 451, 2005.

[4] B. D. Scott *New Journal of Physics*, vol. 7, p. 92, 2005.

[5] K. Itoh, S.-I. Itoh, P. H. Diamond, A. Fujisawa, M. Yagi, T. Watari, Y. Nagashima, and A. Fukuyama *Plasma and Fusion Research*, vol. 1, p. 037, 2006.

[6] P. H. Diamond, S.-I. Itoh, K. Itoh, and T. S. Hahm *Plasma Physics and Controlled Fusion*, vol. 47, p. R35, 2005.

[7] N. Chakrabarti, P. N. Guzdar, R. G. Kleva, V. Naulin, J. J. Rasmussen, and P. K. Kaw *Physics of Plasmas*, vol. 15, p. 112310, 2008.

[8] R. Singh, A. Storelli, O. D. Gürcan, P. Hennequin, L. Vermare, P. Morel, and R. Singh *Plasma Physics and Controlled Fusion*, vol. 57, p. 125002, 2018.

[9] Z. Qiu, L. Chen, and F. Zonca *Plasma Science and Technology*, vol. 20, p. 094004, 2018.

[10] h. S. Zhang and Z. Lin *Physics of Plasmas*, vol. 17, p. 072502, 2010.

[11] L. Wang, J. Q. Dong, Y. Shen, and H. D. He *Plasma Physics and Controlled Fusion*, vol. 53, p. 095014, 2011.

[12] I. Novikau, A. Biancalani, A. Bottino, G. D. Conway, O. D. Gürcan, P. Manz, P. Morel, E. Poli, and A. Di Siena *Physics of Plasmas*, vol. 24, p. 122117, 2017.

[13] C. Ehrlacher, X. Garbet, V. Grandgirard, Y. Sarazin, P. Donnel, E. Caschera, P. Ghendrih, and D. Zarzoso *Journal of Physics: Conference Series*, vol. 1125, p. 012010, 2018.

[14] V. Grandgirard, X. Garbet, C. Ehrlacher, A. A. Biancalani, A. Bottino, I. Novikau, Y. Asahi, E. Caschera, G. Dif-Pradalier, D. P, *et al. Physics of Plasmas*, vol. 26, p. 122304, 2019.

[15] I. Novikau, A. Biancalani, A. Bottino, P. Lauber, P. Manz, E. Poli, G. D. Conway, A. Di Siena, N. Ohana, E. Lanti, *et al. Physics of Plasmas*, vol. 27, p. 042512, 2020.

[16] X. Q. Xu, Z. Xiong, Z. Gao, W. M. Nevins, and G. R. McKee *Physical Review Letters*, vol. 100, p. 215001, 2008.

[17] L. Feng, Z. Lin, J. Q. Dong, and K. J. Zhang *Physics of Plasmas*, vol. 17, p. 112318, 2010.

[18] P. Niskala, T. P. Kiviniemi, L. S, and T. Korpilo *Nuclear Fusion*, vol. 55, p. 073012, 2015.

[19] A. Storelli, L. Vermare, P. Hennequin, O. D. Gürcan, G. Dif-Predalier, Y. Sarazin, X. Garbet, T. Görler, R. Singh, P. Morel, *et al. Plasma Physics and Controlled Fusion*, vol. 57, p. 125002, 2018.

[20] A. Biancalani, A. Bottino, C. Ehrlacher, V. Grandgirard, G. Merlo, I. Novikau, Z. Qiu, E. Sonnendrücker, X. Garbet, and T. Görler *Physics of Plasmas*, vol. 24, p. 062512, 2017.

[21] A. Di Siena, A. Biancalani, T. Görler, H. Doerk, I. Novikau, P. Lauber, A. Bottino, and E. Poli *Nuclear Fusion*, vol. 58, p. 106014, 2018.

[22] M. Jakubowski, R. J. Fonck, and G. R. McKee *Physical Review Letters*, vol. 89, p. 265003, 2002.

[23] A. Krämer-Flecken, S. Soldatov, H. R. Koslowski, and O. Zimmermann *Physical Review Letters*, vol. 97, p. 045006, 2006.

[24] A. Fujisawa *Nuclear Fusion*, vol. 49, p. 013001, 2009.

[25] G. D. Conway, A. Angioni, F. Ryter, P. Sauter, and J. Vicente *Physical Review Letters*, vol. 106, p. 065001, 2011.

[26] G. S. Xu, B. N. Wan, H. Q. Wang, H. Y. Guo, H. L. Zhao, A. D. Liu, V. Naulin, P. H. Diamond, G. R. Tynan, M. Xu, *et al. Physical Review Letters*, vol. 107, p. 125001, 2011.

[27] J. C. Hillesheim, W. A. Peebles, T. A. Carter, L. Schmitz, and T. L. Rhodes *Physics of Plasmas*, vol. 19, p. 022301, 2012.

[28] L. Vermare, P. Hennequin, and O. D. Gürcan *Nuclear Fusion*, vol. 52, p. 063008, 2012.

[29] C. A. De Meijere, S. Coda, Z. Huang, L. Vermare, T. Vernay, V. Vuille, S. Brunner, J. Dominski, P. Hennequin, A. Krämer-Flecken, *et al. Nuclear Fusion*, vol. 49, p. 075002, 2009.

[30] A. V. Melnikov, L. G. Eliseev, S. V. Perfilov, S. E. Lysenko, R. V. Shurygin, V. N. Zenin, G. S. A, L. I. Krupnik, A. S. Kozachek, R. Y. Solomatin, *et al. Nuclear Fusion*, vol. 55, p. 063001, 2015.

[31] H. Sugama and T.-H. Watanabe *Journal of Plasma Physics*, vol. 72, p. 825, 2006. Erratum vol. 74, p. 139, 2007.

[32] F. Zonca and L. Chen *Europhysics Letters*, vol. 83, p. 35001, 2008.

[33] A. I. Smolyakov, M. F. Bashir, A. G. Efimov, M. Yagi, and N. Miyato *Plasma Physics Reports*, vol. 42, p. 407, 2016.

[34] R. Hager and K. Hallatschek *Physics of Plasmas*, vol. 16, p. 072503, 2009.

[35] Z. Qiu, F. Zonca, and L. Chen *Plasma Science and Technology*, vol. 13, p. 257, 2011.

[36] F. Palermo, E. Poli, A. Bottino, A. Biancalani, G. D. Conway, and B. Scott *Physics of Plasmas*, vol. 24, p. 072503, 2017.

[37] F. Palermo, E. Poli, and A. Bottino *Physics of Plasmas*, vol. 27, p. 032507, 2020.

[38] M. Sasaki, K. Itoh, T. Kobayashi, N. Kasuya, A. Fujisawa, and S.-I. Itoh *Nuclear Fusion*, vol. 58, p. 112005, 2018.

[39] Z. Qiu, L. Chen, and F. Zonca *Plasma Physics and Controlled Fusion*, vol. 51, p. 012001, 2009.

[40] E. Mazzucato *Physics of Fluids B*, vol. 1, p. 1855, 1989.

[41] S. Nowak and A. Orefice *Physics of Fluids B*, vol. 5, p. 1993, 1993.

[42] D. Farina *Fusion Science and Technology*, vol. 52, p. 154, 2007.

[43] G. V. Pereverzev *Reviews of Plasma Physics*, vol. 19, p. 1, 1996.

[44] G. V. Pereverzev *Physics of Plasmas*, vol. 5, p. 3529, 1998.

[45] N. Bertelli, O. Maj, E. Poli, R. Harvey, J. C. Wright, P. T. Bonoli, C. K. Phillips, A. P. Smirnov, E. Valeo, and J. R. Wilson *Physics of Plasmas*, vol. 19, p. 082510, 2012.

[46] E. Poli, A. Bock, M. Lochbrunner, O. Maj, M. Reich, A. Snicker, A. Stegmeir, F. Volpe, N. Bertelli, R. Bilato, *et al. Computer Physics Communications*, vol. 225, p. 36, 2018.

[47] Z. X. Lu, F. Zonca, and A. Cardinali *Physics of Plasmas*, vol. 19, p. 042104, 2012.

[48] Z. X. Lu, F. Zonca, and A. Cardinali *Physics of Plasmas*, vol. 20, p. 032115, 2013.

[49] Z. X. Lu *Physics of Plasmas*, vol. 22, p. 052118, 2015.

[50] G. V. Pereverzev *Physics of Plasmas*, vol. 8, p. 3664, 2001.

[51] F. Palermo, A. Biancalani, C. Angioni, F. Zonca, and A. Botitno *Europhysics Letters*, vol. 115, p. 15001, 2016.

[52] A. Biancalani, F. Palermo, C. Angioni, A. Bottino, and F. Zonca *Physics of Plasmas*, vol. 23, p. 112115, 2016.

[53] E.-M. Graefe and R. Schubert *Physical Review A*, vol. 83, p. 060101(R), 2011.

[54] E.-M. Graefe and R. Schubert *Journal of Physics A: Mathematical and Theoretical*, vol. 45, p. 244033, 2012.

[55] S. Jolliet, A. Bottino, P. Angelino, R. Hatzky, T. M. Tran, B. F. McMillan, O. Sauter, K. Appert, Y. Idomura, and L. Villard *Computer Physics Communications*, vol. 177, p. 409, 2007.

[56] A. Bottino and E. Sonnendrücker *Journal of Plasma Physics*, vol. 81, p. 435810501, 2015.

[57] E. Lanti, N. Ohana, N. Tronko, T. Hayward-Schneider, A. Bottino, B. F. McMillan, A. Mishchenko, A. Scheinberg, A. Biancalani, P. Angelino, *et al. Computer Physics Communications*, p. submitted, 2020.

[58] R. G. Littlejohn *Physics Reports*, vol. 138, p. 193, 1986.

[59] H. Weber, O. Maj, and E. Poli *Journal of Physics: Conference Series*, vol. 1125, p. 012022, 2018.

[60] G. Manfredi and M. R. Feix *Physical Review E*, vol. 62, p. 4665, 2000.

[61] E. Poli, G. V. Pereverzev, and A. G. Peeters *Physics of Plasmas*, vol. 6, p. 5, 1999.

[62] R. Sugihara and H. Shamoto *Physics Letters A*, vol. 280, p. 340, 2001.

[63] M. Bornatici and O. Maj *Plasma Physics and Controlled Fusion*, vol. 45, p. 707, 2003.

[64] G. D. Conway, C. Tröster, B. D. Scott, and K. Hallatschek *Plasma Physics and Controlled Fusion*, vol. 50, p. 055009, 2008.

[65] G. Wang, W. A. Peebles, T. L. Rhodes, M. E. Austin, Z. Yan, G. R. McKee, R. J. La Haye, K. H. Burrell, E. J. Doyle, J. C. Hillesheim, *et al. Physics of Plasmas*, vol. 20, p. 092501, 2013.

[66] V. P. Lakhin, E. A. Sorokina, V. I. Ilgisonis, and L. V. Konovaltseva *Plasma Physics Reports*, vol. 41, p. 975, 2015.

[67] M. Sasaki, K. Itoh, A. Ejiri, and Y. Takase *Contributions to Plasma Physics*, vol. 48, p. 68, 2008.

[68] G. Merlo, S. Brunner, Z. Huang, S. Coda, T. Görler, L. Villard, A. Bañon Navarro, J. Dominski, M. Fontana, F. Jenko, *et al. Nuclear Fusion*, vol. 60, p. 034003, 2018.

[69] L. Villard, B. F. McMillan, E. Lanti, N. Ohana, A. Bottino, A. Biancalani, I. Novikau, S. S. Brunner, O. Sauter, N. Tronko, and A. Mishchenko *Plasma Physics and Controlled Fusion*, vol. 61, p. 034003, 2019.

[70] D. E. Ruiz, M. E. Glinsky, and I. Y. Dodin *Journal of Plasma Physics*, vol. 85, 2019.

[71] I. Y. Dodin, D. E. Ruiz, K. Yanagihara, Y. Zhou, and S. Kubo *Physics of Plasmas*, vol. 26, p. 072110, 2019.

[72] E.-M. Graefe, A. Rush, and R. Schubert *IEEE Journal of Selected Topics in Quantum Electronics*, vol. 22, p. 500906, 2016.

[73] G. Agrawal, *Nonlinear Fiber Optics, 6th Ed.* Academic Press, 2019.

[74] D. L. Mills, *Nonlnear Optics*. Berlin Heidelberg: Springer, 1991.

[75] B. Hall, M. Lisak, D. Anderson, R. Fedele, and V. E. Semenov *Physical Review E*, vol. 65, p. 035602(R), 2002.

[76] H. Liu and E. Tadmor *Methods and Applications of Analysis*, vol. 9, p. 517, 2002.

[77] D. V. Dylov and J. W. Fleischer *Physical Review Letters*, vol. 100, p. 103903, 2008.

[78] F. Zonca and L. Chen *Physics of Plasmas*, vol. 21, p. 072120, 2014.

[79] F. Zonca and L. Chen *Physics of Plasmas*, vol. 21, p. 072121, 2014.

[80] F. Zonca, L. Chen, S. Briguglio, G. Fogaccia, A. V. Milovanov, Z. Qiu, G. Vlad, and X. Wang *Plasma Physics and Controlled Fusion*, vol. 57, p. 014024, 2015.

[81] L. Chen and F. Zonca *Revirew of Modern Physics*, vol. 88, p. 015008, 2016.

[82] W. van Saarlos and P. C. Hohenberg *Physica*, vol. 56D, p. 303, 1992.

[83] V. García-Morales and K. Krischer *Contemporary Physics*, vol. 53, p. 79, 2012.

[84] S. W. McDonald *Physics Reports*, vol. 158, p. 337, 1988.

[85] I. B. Bernstein *Physics of Fluids*, vol. 18, p. 320, 1975.

[86] A. Bravo-Ortega and A. H. Glasser *Physics of Fluids B*, vol. 3, p. 529, 1991.

[87] K. Hepp *Communications in Mathematical Physics*, vol. 35, p. 265, 1974.

[88] E. J. Heller *Journal of Chemical Physics*, vol. 62, p. 1544, 1975.